Electronic Supplementary Material (ESI) for Journal of Materials Chemistry A.

Supporting Information

Ultrathin VO_2 Nanosheets Self-Assembled into 3D Micro/Nano-Structured Hierarchical Porous Sponge-Like Micro-Bundles for Long-Life and High-Rate Li-Ion Batteries

Pengcheng Liu,[a,d]* Yuan Xu,[a,d] Kongjun Zhu,[a]* Kan Bian,[a] Jing Wang,[a] Xu Sun,[a]

Guo`an Tai,[a] Yanfeng Gao,[b] Hongjie Luo,[b] Li Lu,[c] Jinsong Liu[d]

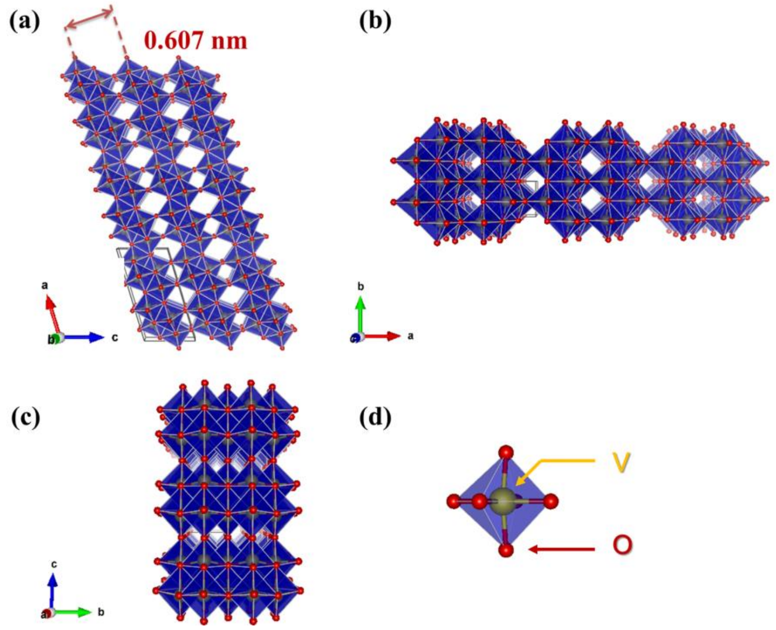

Figure S1. Crystal structure model of VO_2 (B) viewed along the [010] (a), [001] (b), and [100] (c) directions; (d) VO_6 octahedron which is the building blocks of VO_2 (B) crystal structure.

Discussion:

VO_2 (B) belongs to monoclinic C2/m space group. Its crystal structure is constructed by stacking of V_4O_{10} layers, leading to form abundant tunnels. Moreover, Figure S1a shows that the interlayer space of (001) is 0.607 nm.

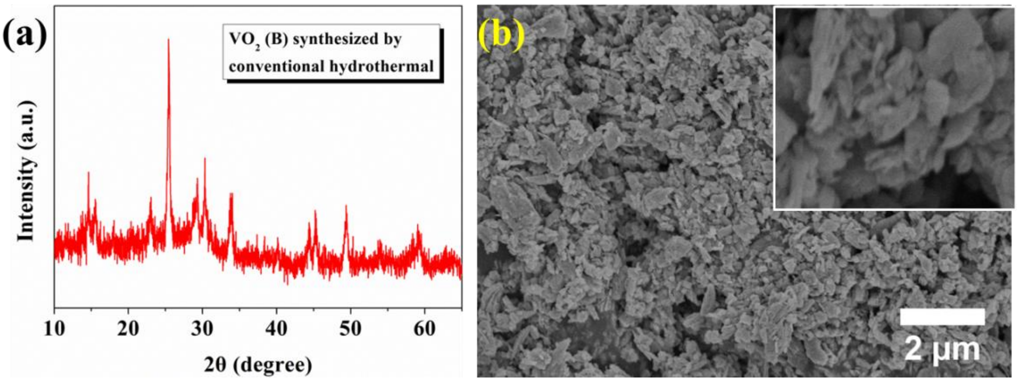

Figure S2. Characterizations of VO_2 (B) synthesized by conventional hydrothermal. (a) XRD pattern; (b) SEM image.

Discussion:

It can be seen that the XRD pattern of VO_2 (B) nanoribbons (Figure 1BI) shows a stronger peak intensity and smaller full width at half maximum (FWHM) than that of VO_2 (B) synthesized by conventional hydrothermal (Figure S2a). This result means that VO_2 (B) nanoribbons synthesized by HTMM possess a better crystallinity. Furthermore, compared with VO_2 (B) nanoribbons, the morphology of VO_2 (B) synthesized by conventional hydrothermal is very irregular and small nanoparticles (Figure S2b). This SEM result also means that VO_2 (B) nanoribbons synthesized by HTMM possess a better crystallinity, which agrees well with the result of XRD. These results reveal well that HTMM can greatly improve the crystallinity of products.

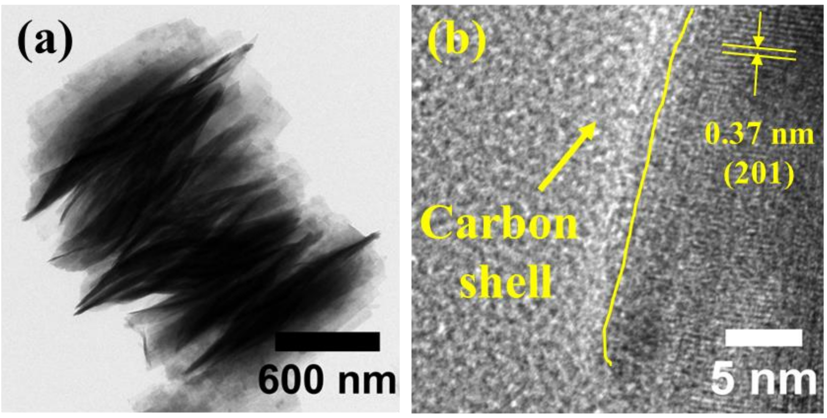

Figure S3. Morphology observation of VO_2 (B)@C-SLMBs. (a) TEM image; (b) HRTEM image.

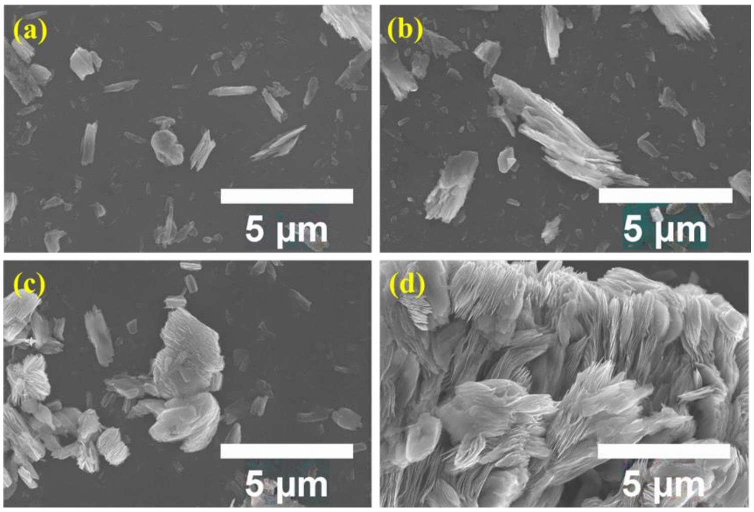

Figure S4. Morphology evolution of VO_2 (B)@C-SLMBs prepared by HTMM at 240 ℃ for different time when the molar ratio of glucose: V_2O_5 is 1. (a) 10 min; (b) 30 min; (c) 1 h; (d) 6 h.

Discussion:

It can be seen clearly that these nanosheets become larger and larger, and the layer number of micro-bundles become more and more with time increasing, which reveals that the growth of VO_2 (B)@C-SLMBs is the self-assembly process based on the oriented attachment mechanism.[1, 2]

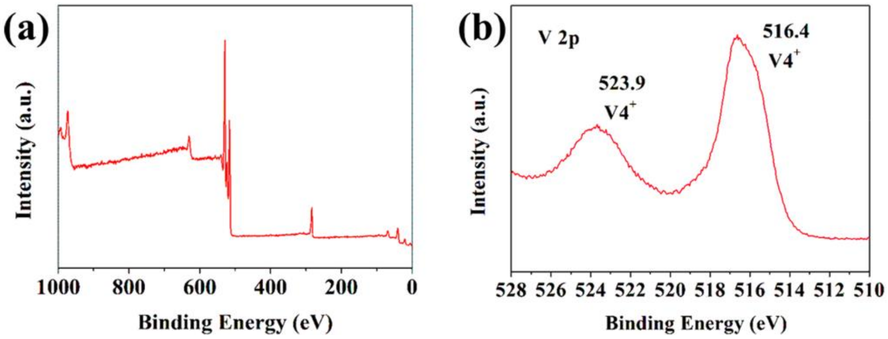

Figure S5. XPS spectrums of VO_2 (B)@C-SLMBs. (a) Survey XPS spectrum; (b) XPS spectrum of core level V 2p.

Discusion:

Valence states and bounding types of elements in VO_2 (B)@C-SLMBs are further identified by XPS. The typical survey XPS spectrum for VO_2 (B) is presented in Figure S5a. For the V 2p spectrum (Figure S5b), the peaks of V 2p3/2 and V 2p1/2 are 516.4 and 523.9 eV, corresponding to V^{4+} (516.0 and 524.1 eV).[3]

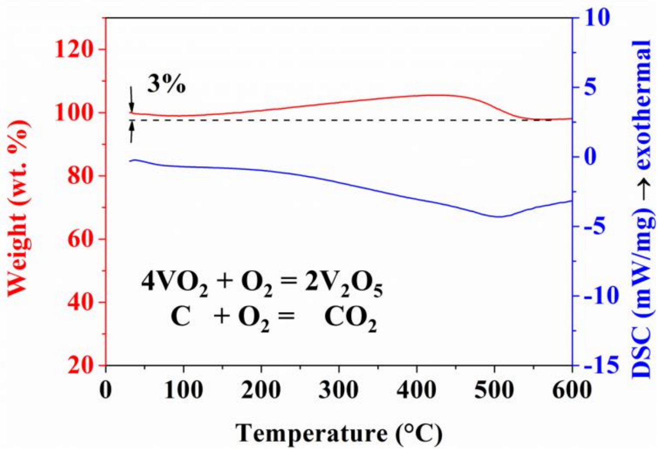

Figure S6. TG/DSC curves of VO_2 (B)@C-SLMBs, which were conducted under air.

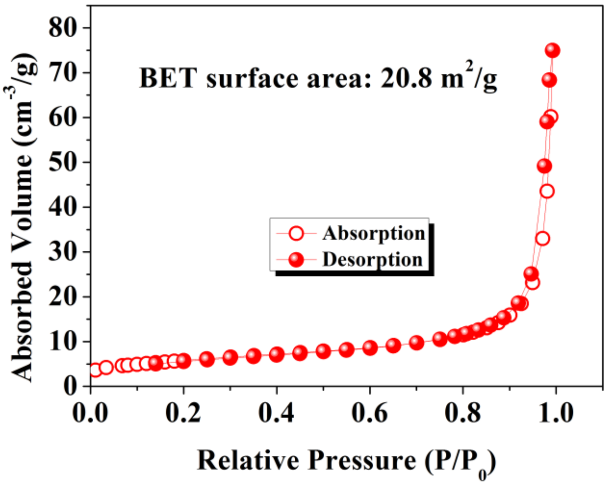

Figure S7. Nitrogen adsorption-desorption isotherm of low-dimensional VO_2 (B) nanoribbons.

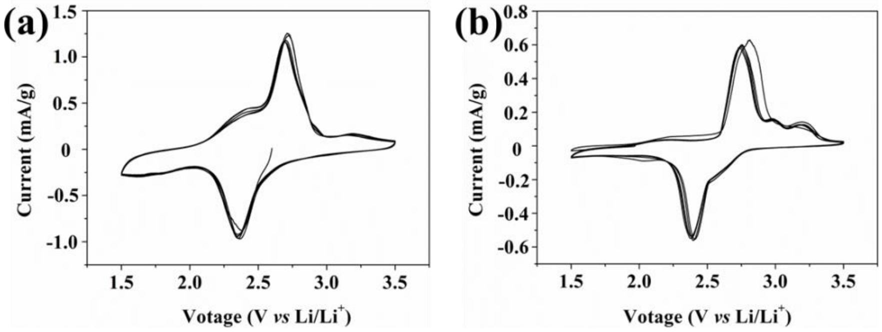

Figure S8. CV curves with the first five cycles of (a) VO_2 (B)@C-SLMBs and (b) VO_2 (B) nanoribbons at a scanning rate of 0.5 mV/s in the voltage range from 3.5~1.5 V (*vs.* Li/Li$^+$)

Discussion:

Figure S8a shows the CV curves of VO_2 (B)@C-SLMBs. A obvious pair of redox peaks occur, in which the cathodic peak locates at ~2.69 V, and the anode peak locates at ~2.41 V. Importantly, compared with that of VO_2 (B) nanoribbons (Figure S8b), the CV curves of VO_2 (B)@C-SLMBs are better overlapped, which also indicates that VO_2 (B)@C-SLMBs possess the higher reversibility and better capacity retention.[4] Furthermore, it can also be observed that the CV curves area of VO_2 (B)@C-SLMBs is larger than that of VO_2 (B) nanoribbons, which also suggests that 3D VO_2 (B)@C-SLMBs exhibit higher capacity.

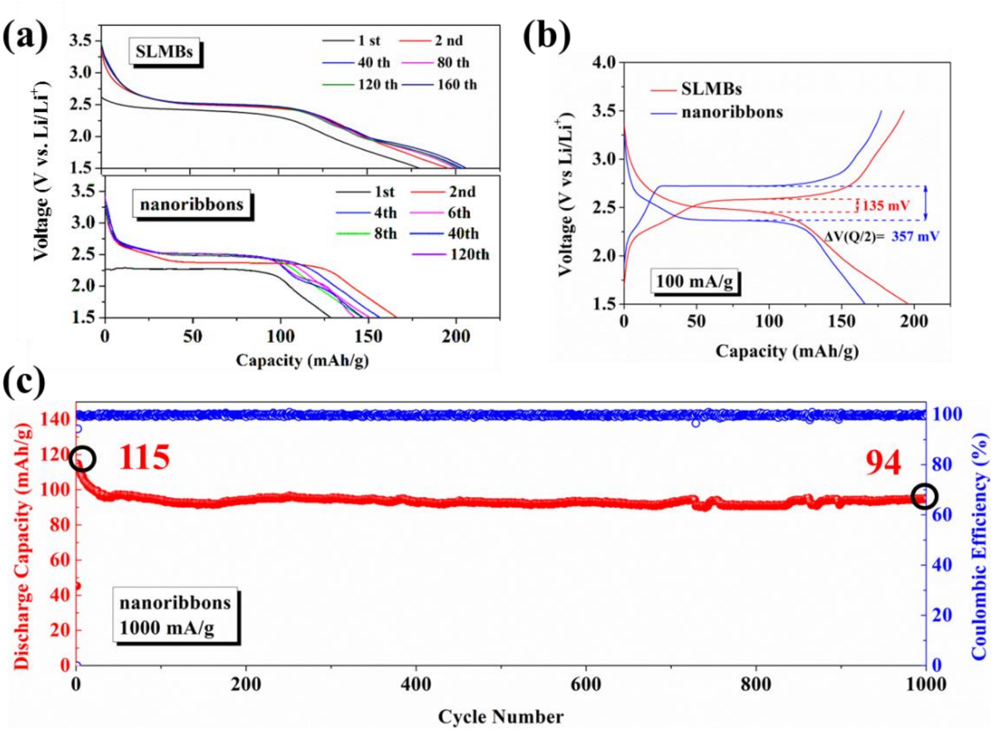

Figure S9. Electrochemical measurements of 3D hierarchical porous VO_2 (B)@C-SLMBs and low-dimensional VO_2 (B) nanoribbons. (a) Discharge curves of SLMBs and nanoribbons at the current density of 100 mA/g; (b) the second charge-discharge curve of SLMBs and nanoribbons at 100 mA/g; (c) long cycling performance of nanoribbons at a large current density of 1000 mA/g.

Discusion:

Figure S9a shows the discharge patterns of 3D hierarchical porous VO_2 (B)@C-SLMBs and low-dimensional VO_2 (B) nanoribbons. It can be seen that discharge curves of VO_2 (B)@C-SLMBs are well overlapped. However, the discharge capacity of VO_2 (B) nanoribbons is becoming lower and lower without good overlapped discharge curves. This reveals that VO_2 (B)@C-SLMBs have the higher reversibility and better capacity retention. The overpotential is measured from the difference between charge and discharge potential at the half reversible capacity, noted as $\Delta V(Q/2)$.[5, 6] The overpotential of VO_2 (B)@C-SLMBs is only 135 mV, which is much lower than 357 mV of VO_2 (B) nanoribbons (Figure S9b), showing higher electrical and ionic conductivity of VO_2 (B)@C-SLMBs. Figure S9c shows the long-life cycling of VO_2 (B) nanoribbons at 1000 mA/g. Its second capacity is 115 mAh/g. And, the capacity decreases quickly during the following cycles. After 1000 cycles, the capacity of 94 mAh/g can only be kept.

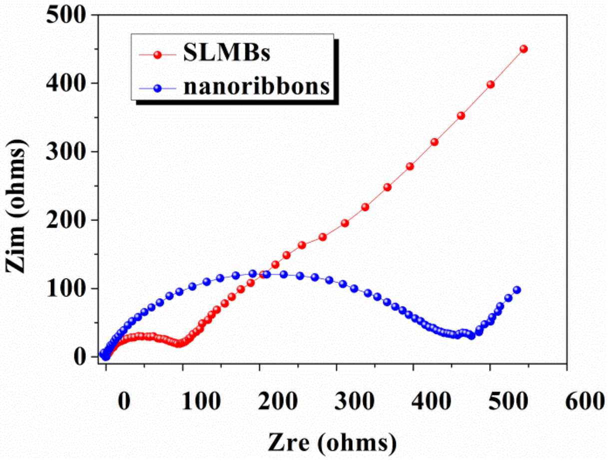

Figure S10. Comparison of electrochemical impedance spectroscopy pattern of VO_2 (B)@C-SLMBs and VO_2 (B) nanoribbons after long-tern cycling.

Table S1 Comparison of electrochemical performances between the present 3D hierarchical porous VO_2 (B)@C-SLMBs and other cathode materials for LIBs

Cathode materials	**Capacity retention at a small current (cycle number, final capacity)**	**Capacity retention at a large current (cycle number, final capacity)**	**Rate capability [a] (recovery ratio [b])**
3D hierarchical porous VO_2 (B)@-SLBMs (our work)	105% at 100 mA/g (160, 206 mAh/g)	104% at 1000 mA/g (1000, 142 mAh/g)	100 mAh/g at 3000 mA/g (104%)
VO_2 (B) nanorods[7]	49% at 100 mA/g (17, 75 mAh/g)	NA	NA
VO_2 (B)@C nanobelts[8]	80% at 100 mA/g (50, 128 mAh/g)	NA	100 mAh/g at 2000 mA/g (NA)
VO_2 (B)/C nanobelts[9]	70%.6 at 50 mA/g (100, 152 mAh/g)	NA	138 mAh/g at 1000 mA/g (75.7%)
Nanoscoll buffered Hybrid nanostructural VO_2 (B)[6]	85% at 100 mA/g (100, 134 mAh/g)	82% at 1000 mA/g (1000, 96 mAh/g)	98 mAh/g at 2000 mA/g (98.7%)
3D GO-VO_2 (B) nanosheet flowers[10]	60% at 50 mA/g (50, 252 mAh/g)	NA	102 mAh/g at 5000 mA/g (NA)
micro/nano-structured VO_2 (B) mesocrystals[11]	74% at 150 mA/g (50, 190 mAh/g)	NA	158 mAh/g at 1500 mA/g (74%)
VO_2 (B)-rGO composites[12]	74% at 20 mA/g (100, 85 mAh/g)	NA	NA
VO_2 (B) hollow microspheres[5]	90% at 100 mA/g (100, 181 mAh/g)	73% at 1000 mA/g (1000, 104 mAh/g)	129 mAh/g at 2000 mA/g (93%)
VO_2 (B) nanobelts[2]	83% at 100 mA/g	NA	90 mAh/g at 2000

	(100, 121 mAh/g)		mA/g (98%)
Carbon fiber cloth@ VO_2 (B)[4]	95% at 100 mA/g (100, 138 mAh/g)	90% at 1000 mA/g (200, 117 mAh/g)	91 mAh/g at 2000 mA/g (98)
Cucumber-like V_2O_5/PEDOT&MnO_2[13]	93% at 50 mA/g (40, 166 mAh/g)	70% at 100 mA/g (200, 110 mAh/g)	48 mAh/g at 500 mA/g (90%)
Single-crystal $LiMn_2O_4$ nanotubes[14]	89% at 15 mA/g (8, 105 mAh/g)	70% at 750 mA/g (1500, 70 mAh/g)	80 mAh/g at 1500 mA/g (NA)
Heterostructure $LiMn_2O_4$ [15]	85% at 150 mA/g (100, 102 mAh/g)	NA	88 mAh/g at 1300 mA/g (100%)
Binder-free $LiCoO_2$/C nanotubes[16]	95% at 14 mA/g (50, 144 mAh/g)	NA	137.4 mAh/g at 280 mA/g (NA)
Electrospinning $LiFePO_4$ nanowires[17]	95% at 170 mA/g (100, 161 mAh/g)	NA	93 mAh/g at 1700 mA/g (100%)

[a] Rate capability in this section refers to the discharge specific capacity delivered at the largest current density.

[b] Recovery rate in this section refers to the ratio of the discharge capacity recovered when the current returns back to a small one to the corresponding initial capacity.

Reference

1. P. Liu, K. Zhu, Y. Gao, Q. Wu, J. Liu, J. Qiu, Q. Gu and H. Zheng, *CrystEngComm*, 2013, **15**, 2753-2760.
2. L. Li, P. Liu, K. Zhu, J. Wang, J. Liu and J. Qiu, *J. Mater. Chem. A*, 2015, **3**, 9385-9389.
3. Y.-L. Ding, Y. Wen, C. Wu, P. A. van Aken, J. Maier and Y. Yu, *Nano Lett.*, 2015, **15**, 1388-1394.
4. S. Li, G. Liu, J. Liu, Y. Lu, Q. Yang, L.-Y. Yang, H.-R. Yang, S. Liu, M. Lei and M. Han, *J. Mater. Chem. A*, 2016, **4**, 6426-6432.
5. C. Niu, J. Meng, C. Han, K. Zhao, M. Yan and L. Mai, *Nano Lett.*, 2014, **14**, 2873-2878.
6. L. Mai, Q. Wei, Q. An, X. Tian, Y. Zhao, X. Xu, L. Xu, L. Chang and Q. Zhang, *Adv. Mater.*, 2013, **25**, 2969-2973.
7. C. V. Subba Reddy, E. H. Walker, S. A. Wicker, Q. L. Williams and R. R. Kalluru, *Current Applied Physics*, 2009, **9**, 1195-1198.
8. X. Rui, D. Sim, C. Xu, W. Liu, H. Tan, K. Wong, H. H. Hng, T. M. Lim and Q. Yan, *RSC Adv.*, 2012, **2**, 1174-1180.
9. Q. Zhao, L. Jiao, W. Peng, H. Gao, J. Yang, Q. Wang, H. Du, L. Li, Z. Qi, Y. Si, Y. Wang and H. Yuan, *J. Power Sources*, 2012, **199**, 350-354.
10. C. Nethravathi, C. R. Rajamathi, M. Rajamathi, U. K. Gautam, X. Wang, D. Golberg and Y. Bando, *ACS Appl. Mater. Interfaces*, 2013, **5**, 2708-2714.
11. E. Uchaker, M. Gu, N. Zhou, Y. Li, C. Wang and G. Cao, *Small*, 2013, **9**, 3880-3886.
12. H. Zhao, L. Pan, S. Xing, J. Luo and J. Xu, *J. Power Sources*, 2013, **222**, 21-31.
13. L. Mai, F. Dong, X. Xu, Y. Luo, Q. An, Y. Zhao, J. Pan and J. Yang, *Nano Lett.*, 2013, **13**, 740-745.
14. Y.-L. Ding, J. Xie, G.-S. Cao, T.-J. Zhu, H.-M. Yu and X.-B. Zhao, *Adv. Funct. Mater.*, 2011, **21**, 348-355.
15. M. J. Lee, S. Lee, P. Oh, Y. Kim and J. Cho, *Nano Lett.*, 2014, **14**, 993-999.
16. S. Luo, K. Wang, J. Wang, K. Jiang, Q. Li and S. Fan, *Adv. Mater.*, 2012, **24**, 2294-2298.
17. C. Zhu, Y. Yu, L. Gu, K. Weichert and J. Maier, *Angew. Chem. Int. Ed. Engl.*, 2011, **50**, 6278-6282.